Computational Modeling of Spatially Selective Retinal Stimulation With Temporally Interfering Electric Fields

Xiaofan Su, Jiahui Guo, Meixuan Zhou, Jianpin Chen, Liming Li, Yao Chen, Xiaohong Sui, *Member, IEEE*, Heng Li, and Xinyu Chai

***Abstract*— Retinal electrical stimulation is a widely utilized method to restore visual function for patients with retinal degenerative diseases. Transcorneal electrical stimulation (TES) represents an effective way to improve the visual function due to its potential neuroprotective effect. However, TES with single electrode fails to spatially and selectively stimulate retinal neurons. Herein, a computational modeling method was proposed to explore the feasibility of spatially selective retinal stimulation via temporally interfering electric fields. An eyeball model with multiple electrodes was constructed to simulate the interferential electric fields with various electrode montages and current ratios. The results demonstrated that the temporal interference (TI) stimulation would gradually generate an increasingly localized high-intensity region on retina as the return electrodes moved towards the posterior of the eyeball and got closer. Additionally, the position of the convergent region could be modulated by regulating the current ratio of different electrode channels. The TI strategy with multisite and steerable stimulation can stimulate local retinal region with certain convergence and a relatively large stimulation range, which would be a feasible approach for the spatially selective retinal neuromodulation.**

***Index Terms*— Computational modeling, retinal neuromodulation, spatial selectivity, temporal interference, transcorneal electrical stimulation.**

I. Introduction

TRANSCORNEAL electrical stimulation (TES) is a widely adapted retinal neuromodulation strategy that delivers electrical currents to the retina via contact lens electrodes attached to the corneal surface [1]–[3]. Chow *et al.* firstly demonstrated that the subthreshold electrical stimulation of the retina could be a potential therapy for retinitis pigmentosa [4]. Later, evolving researches proved that TES might become a promising therapeutic strategy to facilitate the visual restoration [5]–[7] and improve the survival of retinal cells [5], [8], [9] against several ophthalmic diseases and disorders. This can be attributed to its potential neurotrophic effects induced by electrical stimulation [8], [10]. Meanwhile, TES can effectively active visual cortex response related to the reported phosphene percept [11], [12]. In addition, it can evaluate the retinal function by estimating the residual function of the inner retinal layer by the threshold current for evoking phosphenes [12]. Thus, it can be utilized to preoperatively screen suitable candidates for implanting of retinal prostheses clinically [13], [14]. Until now, two types of electrodes have been commonly used in TES, which are electroretinography (ERG)-Jet electrodes and Dawson-trick-Litzkow (DTL)-Plus electrodes [1]. Xie *et al.* demonstrated that DTL-Plus electrodes-based TES preferentially activated the inferior, nasal, peripheral retina, whereas ERG-Jet electrodes-based TES activated more extensive peripheral, nasal hemiretina [11]. However, if TES can activate certain specific region of retina versus peripheral retinas, it will be a more ideal strategy to treat ophthalmic diseases and evaluate retinal viability [11].

Electrical stimulation based on interferential electric fields is produced by simultaneous application of two sinusoidal currents with slightly different frequencies through different electrode channels to generate temporal interference (TI) patterns [15]. Previous study has demonstrated that neurons near the electrodes were not stimulated despite stimulation of neurons deeper in the tissue [16]. Therefore, TI stimulation has been utilized as an electrotherapy method for the neuromodulation of the peripheral nerve system [17], and a noninvasive deep brain stimulation strategy for the central nerves system [18].

However, few studies applied interferential electric fields in the retinal neuromodulation, which exhibited great potential in the extraocular electrical stimulation of the retina [19], [20]. As mentioned above, TES using a single electrode preferentially activates retinal neurons in the peripheral visual field or directly activates the entire retina, while lacking the ability to selectively modulate retinas [11]. Besides, it is

Manuscript received October 29, 2020; revised January 11, 2021; accepted January 25, 2021. Date of publication January 28, 2021; date of current version March 2, 2021. This work was supported in part by the National Natural Science Foundation of China under Grant 62073221, Grant 61773256, Grant 61971280, Grant 61773259, and Grant 81671801; and in part by the Project funded by China Postdoctoral Science Foundation under Grant 2019M661509. *(Xiaofan Su and Jiahui Guo contributed equally to this work.) (Corresponding authors: Xinyu Chai; Heng Li.)*

The authors are with the School of Biomedical Engineering, Shanghai Jiao Tong Universtiy, Shanghai 200240, China (e-mail: suxiaofan228@sjtu.edu.cn; guojiahui@sjtu.edu.cn; liheng@sjtu.edu.cn; xychai@sjtu.edu.cn).

This article has supplementary downloadable material available at https://doi.org/10.1109/TNSRE.2021.3055203, provided by the authors.

Digital Object Identifier 10.1109/TNSRE.2021.3055203

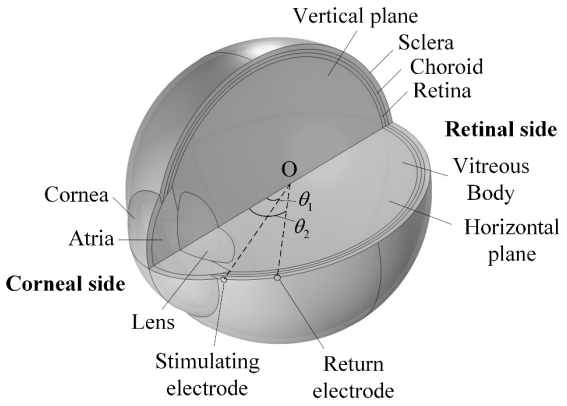

Fig. 1. The electrical conductivity model of the eyeball and the extraocular electrodes. (θ_1 and θ_2 represented the positions of stimulating and return electrodes, respectively.)

possible for TI strategy to spatially and selectively stimulate the localized neurons [21], and further preferentially activate central retinas. Given that, TI electrical stimulation can be applied in spatially selective neuromodulation for retinal impairment patients. Herein, the temporally interfering electric field distributions through modeling is presented. This modeling method simulates current flows with different frequencies from multiple extraocular electrode channels applied to the retina with various electrode montages and current ratios. Moreover, the theoretical convergence and steerability of the electric fields are evaluated. The results could be instructive for the study of a novel retinal neuromodulation method.

II. Methods

A. Electrical Conductivity Model of the Eyeball and Extraocular Electrodes

A 3D electrical conductivity model of the eyeball and multiple extraocular electrodes were constructed in the AC/DC module of COMSOL Multiphysics (COMSOL, Stockholm, SWE). As shown in Fig. 1, the eyeball model contained several basic structures, including cornea, atria, lens, vitreous body (VB), retina, choroid, and sclera [22], [23]. I listed the parameters [23]–[27]. The electric conductivity values of 100 Hz were used. The disc-shaped electrodes had a diameter of 500 μm and a thickness of 50 μm. The eyeball was placed in a 30 mm cube environment full of body fluid with conductivity of 1.5 S/m, which was the same as VB. And Dirichlet boundary conditions were applied both at the interface of electrodes and at the boundary of the cube environment.

B. 2D Electrode Montage and Temporally Interfering Electric Fields

To compare the electric field distribution generated by different electrode placements, 2D and 3D electrode montages were established. In 2D electrode montage, two stimulating channels containing four electrodes were distributed around the eyeball on the horizontal plane. Clearly, as shown in Fig. 2(a), two electrodes placed at the corneal side were defined as stimulating electrodes, and the other two electrodes

TABLE I
Parameters of the Eyeball Model and Extraocular Electrodes

Component	Conductivity (S/m) [24], [25]	Thickness (mm) [23], [26], [27]
Cornea	0.422	0.5
Atria	1.5	2.75
Lens	0.322	4.0
Vitreous body*	1.5	23
Retina	0.5028	0.33
Choroid	0.2779	0.3
Sclera	0.5028	0.45
Body fluid	1.5	-
Electrodes (Pt)	8.9×10^6	-

* The thickness of VB represents the diameter of VB.

placed at retinal side were applied as return electrodes. The first channel was constructed with one stimulating electrode and one return electrode with an alternating sinusoidal current I_1, and the second channel constructed by the rest two electrodes passed the current I_2. The current amplitude from each channel was set as 1 mA. The currents were simultaneously applied to the eye at high frequencies f_1 and $f_2 = f_1 + \Delta f$. (The selection of frequency would be detailed expounded in the *Discussion* section.) At locations where the sinusoidal currents have comparable amplitudes (box i in Fig. 2(b)), superposition of two high-frequency currents with slightly difference frequency Δf produced a waveform that was a high-frequency "carrier wave" (corresponding to the average of the frequencies of two sinusoids, i.e. $(f_1 + f_2)/2$) (black solid line of Fig. 2(c)) modulated by a slow envelope oscillating at the difference frequency Δf (black dotted line). This slow envelope was able to successfully engage neurons.

At locations where the amplitude of one sinusoid dominated than the other, the envelope does not oscillate significantly (box ii in Fig. 2(b)), and the neurons are not fire [20]. The envelope modulation amplitude was calculated under quasi-static conditions [28] using the superposition principle. Fig. 2(b) showed the electric field distribution at an instant in time in which the strength of the total field at any point in space was at its maximum. Analytically, taken y-direction as an example, in all points in space, the strength of the electric field oscillated between $(|E_{1y}| + |E_{2y}|)$ and $||E_{1y}| - |E_{2y}||$ at frequency of Δf, where $|E_{1y}|$ and $|E_{2y}|$ were the peak spatial electric field generated by the first and second electrode pairs, respectively. Thus, the spatial distribution of the envelope modulation amplitude induced by interference along any direction could be calculated [18] based on

$$\left|\vec{E}_{\mathrm{AM}}(\vec{n},\vec{r})\right| = \left|\left|\left(\vec{E}_1(\vec{r}) + \vec{E}_2(\vec{r})\right)\cdot\vec{n}\right| - \left|\left(\vec{E}_1(\vec{r}) - \vec{E}_2(\vec{r})\right)\cdot\vec{n}\right|\right| \quad (1)$$

$\vec{E}_1(\vec{r})$ and $\vec{E}_2(\vec{r})$ represented the electric fields generated by two stimulating channels at the location of $\vec{r}(x,y,z)$ along the direction of $\vec{n}$, which was a unit vector along the direction of interest. The maximal envelop modulation amplitude (MEMA) along any orientation resulted from the superposition of $\vec{E}_1(\vec{r})$ and $\vec{E}_2(\vec{r})$ at the location of $\vec{r}\,(x,y,z)$ was defined

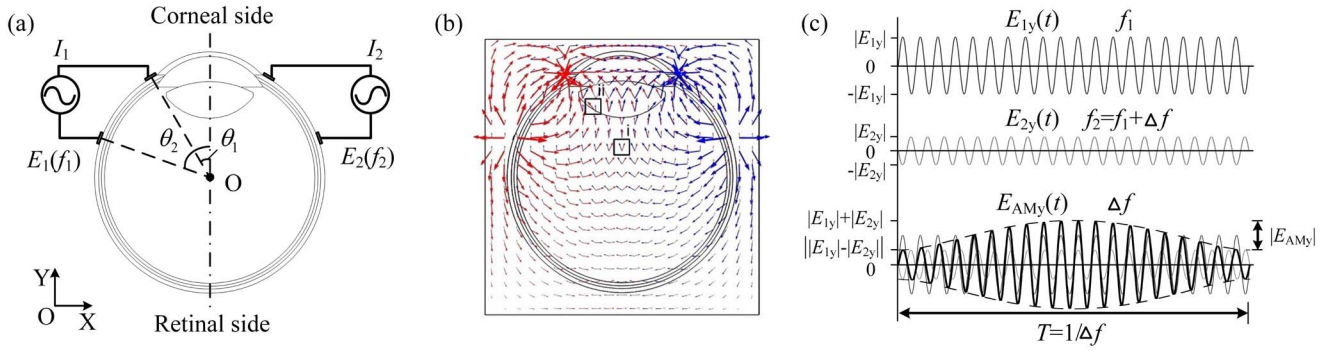

Fig. 2. The diagram of the electrical stimulation via interferential electric fields. (a) The schematic diagram of horizontal plane with two stimulating channels. (b) The electric field lines in the horizontal plane. (c) An example of time-domain waveforms of the applied sinusoidal electric fields in y orientation, $\vec{E}_{1y}(t)$ and $\vec{E}_{2y}(t)$, and modulated interferential electric fields, $\vec{E}_{AMy}(t)$.

as $\vec{E}_{AM-MAX}(\vec{r})$, and could be calculated by (2).

$$\vec{E}_{AM-MAX}(\vec{r}) = \max\left|\vec{E}_{AM}(\vec{n}_1,\vec{r})\right|, \left|\vec{E}_{AM}(\vec{n}_2,\vec{r})\right|, \cdots, \left|\vec{E}_{AM}(\vec{n}_n,\vec{r})\right| \quad (2)$$

During the simulation, there are two pairs of electrodes which were symmetrically distributed on the both side of the eyeball along the longitudinal axis. As shown in Fig. 1 and 2(a), θ_1, θ_2 referred to the angle between the left stimulating electrode, the left return electrode and the longitudinal axis, respectively. In this study, θ_1 was fixed at 30°, indicating that the stimulating electrodes were fixed. θ_2 varied within the range from 50° to 170° with a 20°-step, indicating that the return electrodes were movable from the corneal side to the retinal side. With different electrode placements, MEMAs of horizontal plane and retinal surface were calculated, representing the electric fields originated from the TI stimulation.

In addition, as for a fixed electrode placement, the mobility of the temporally interfering electric fields was evaluated as the ratio of current passing through the stimulating channels change. As mentioned above, I_1 and I_2 referred to the current amplitude passed by the first and second channel, respectively. Given that, as shown in (3), the proportion of I_1 in the total current amplitude was defined as the current ratio α. And when α equaled to 0.5, it revealed that the currents flowing from two channels had the same amplitude but different frequencies. Thus, the total output current of these two channels was 2 mA in total.

$$\alpha = I_1/(I_1 + I_2) \quad (3)$$

C. 3D Electrode Montage and Temporally Interfering Electric Fields

In the 3D electrode montage, four extraocular stimulating channels were formed by two pairs of electrodes on the horizontal plane and the other two pairs on the vertical plane, which were systematically distributed around the eyeball, as shown in Fig. 3. Similarly, the position of the stimulating electrodes by the corneal side was fixed, while the return electrodes were moved from the corneal side to the retinal side. The interferential electric fields generated by 3D electrode

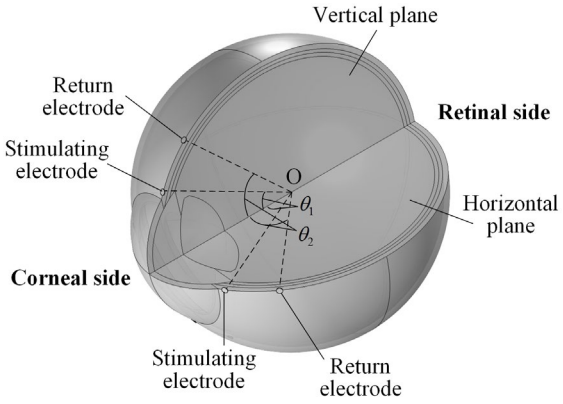

Fig. 3. The schematic diagram of the eyeball model with 3D electrode montage. (θ_1 and θ_2 represented the positions of stimulating and return electrodes, respectively.)

montages were calculated [16] according to

$$\left|\vec{E}_{AM}(\vec{n},\vec{r})\right| = 2\cdot\min\{\vec{E}_1(\vec{r}), \vec{E}_2(\vec{r}), \cdots, \vec{E}_n(\vec{r})\} \quad (4)$$

As for the 3D electrode montage, two current ratios of α_x and α_y represented the current ratio of horizontal and vertical stimulating channels, respectively. They were used to evaluate the steerability of interferential electric fields, as in

$$\alpha_x = I_1/(I_1 + I_2) \quad (5)$$

$$\alpha_y = I_3/(I_3 + I_4) \quad (6)$$

I_3 and I_4 were currents passed by the upper and lower electrode pairs, respectively.

III. Results

A. Temporally Interfering Electric Fields With 2D Electrode Montage

Based on the computational setup, the temporally interfering electric field distributions with different 2D electrode placements were calculated. Firstly, as shown in Fig. 4, MEMAs of the horizontal plane were simulated. The position of return electrodes varied from 50° to 170° with a step of 20°, and values in each step were normalized to 0 to 1. It was found that when the sinusoidal currents were applied to the eyeball model, as θ_2 increased (return electrodes moving from the

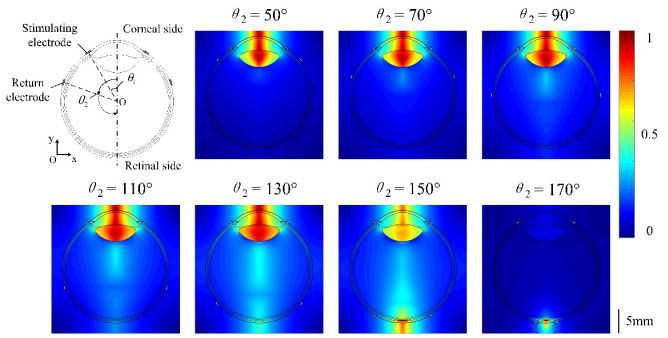

Fig. 4. Normalized interferential electric fields of the horizontal plane with different 2D electrode placements.

corneal side to the retinal side), the maximum site of the electric fields was shifted from the corneal side towards the retinal side. When θ_2 was less than 110°, the strongest electric field appeared within the anterior eye through the cornea, atria, and lens, near the stimulating electrodes. When θ_2 increased to 130°, the electric field intensity of the central retina enhanced, whereas it was still much weaker than that in the anterior region. When θ_2 was 150° and 170°, the maximum electric field was distributed on the retinal side throughout the retinal layer as well as the adjacent choroid and scleral layers, which were close to the return electrodes. The interferential electric fields exhibited favorable penetration and targeted the deep retina.

Furthermore, the electric field distributions of the retinal surface were investigated. The retinal surface referred to the middle layer of the retina in the eyeball model. As shown in Fig. 5, MEMAs of the retinal surface in each position of the return electrode were calculated and normalized from 0 to 1. To analyze the electric field distribution, the 3D hemispherical retinal surface was projected into the XOZ plane and the results were displayed in 3D mesh diagrams on the upper right corner of each illustration of different step. Meanwhile, MEMAs of the horizontal line and vertical line (defined in the first illustration of Fig. 5) were extracted and normalized below the 3D mesh diagram of each illustration. As shown in Fig. 5, MEMAs in the central retina were lower than that in the peripheral retina when θ_2 was less than 90°. The maximal amplitudes of electric fields were distributed in the upper and lower edges (vertical edges) of the retinal surface. When the return electrodes moved towards the retinal side of the eyeball with θ_2 greater than 90°, MEMAs of the central retina were higher than that of the peripheral retina, gradually leading to the formation of a small focal region with strong electric field intensity at the central retina. Based on qualitative analysis, the morphology of the focal region was oval-shape, and its spatial resolution in the horizontal direction was much better than that in the vertical direction. From 1D distribution curves, the electric fields of the vertical line exhibited a wider peak width than that of the horizontal line. It also revealed that the electric field convergence of the horizontal direction was much better than that of the vertical direction.

To evaluate the specific features of the high intensity focal region, MEMAs of horizontal and vertical lines were chosen in Fig. 5 for quantitative analysis. MEMA values of central point, horizontal edge and vertical edge points were shown in Fig. 6(a). As the return electrodes moved closer to the posterior of the eyeball, MEMA values of central point rose significantly, which was corresponding to a quadratic function, compared to the rising trends of horizontal and vertical edges, which were more like linear function. And when θ_2 was greater than 110°, the MEMA of central point was higher than that of edges, resulting in a focal stimulating site with high electric field intensity at the central retina instead of peripheral visual field. Then, to evaluate the spatial resolution of this stimulation strategy, the range of the focal region in central retina was analyzed. The full width at half maxima (50% width) and the full width at 80% maxima (80% width) of the normalized MEMAs from horizontal and vertical lines were calculated, as shown in Fig. 6(b) and 6(c). Values under circumstance that central peak value was greater than the edge values were chosen, whereas values under other cases were masked. The resolution of both horizontal and vertical directions increased with the return electrodes moving closer at the retinal side. When θ_2 equaled to 170°, the 50% width of horizontal and vertical lines was about 12.5° and 23.5°, respectively. Under this electrode placement, the 80% width was about 5.0° in horizontal and 11.5° in vertical. These results also validated that the spatial resolution of interferential electric fields in horizontal direction was much better than that in vertical direction.

Moreover, the influence of different stimulating electrode positions and electrode sizes on the interferential electric fields was evaluated in *Supplementary Information* section A and B, respectively. The results showed that the stimulating electrode position and the electrode size had little impact on the electric field distribution. However, it should be noted that these two parameters might affect the charge injection capability and the safety of the stimulating strategy.

B. Temporally Interfering Electric Fields With 3D Electrode Montage

According to results of the 2D electrode montage, the spatial resolution in the vertical direction was much weaker than that in the horizontal direction. Thus, the 3D electrode montage was constructed by adding two electrode pairs in the vertical plane, which aimed to improve the vertical resolution. In 3D electrode montage, four stimulating channels around the eyeball were formed by eight electrodes. Same as setups in 2D electrode montage, θ_1 was fixed at 30°, θ_2 varied from 50° to 170°. Fig. 7 demonstrated the electric field distributions of the retinal surface. The symmetrical electrode placement contributed to symmetrical electric fields in vertical and horizontal directions. The distributions of MEMAs in the vertical line were identical to that in the horizontal line. Based on the electric field distribution of the retinal surface, the high-intensity range in the 3D electrode montage was square-shaped. Fig. 8 revealed that the best resolution was in both horizontal and vertical direction, whereas the worst resolution was in the diagonal direction. 50% and 80% width in the horizontal and diagonal line were also introduced to evaluate the resolution of different directions (Fig. 8(b) and 8(c)).

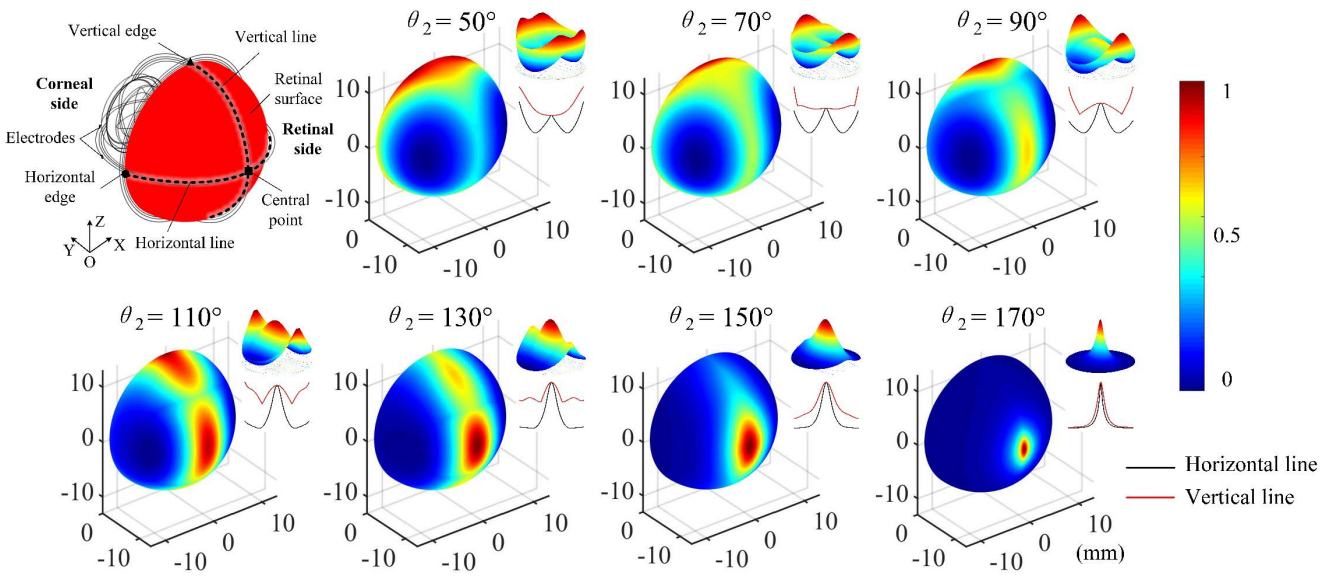

Fig. 5. Normalized interferential electric fields of the retinal surface with 2D different electrode placements. ($\theta_1 = 30°$, θ_2 changed from 50° to 170° with a step of 20°. Upper right: 3D mesh diagrams of MEMAs projected to XOZ plane from retinal surface; lower right: normalized MEMAs of horizontal line and vertical line.)

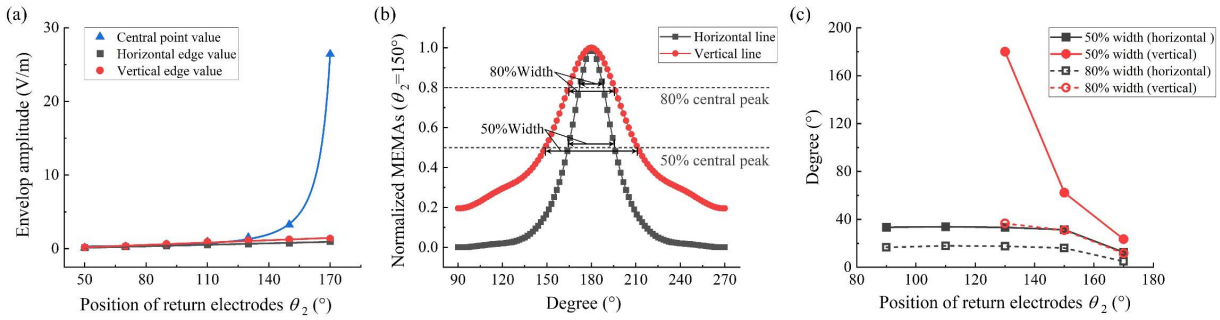

Fig. 6. Quantitative analysis of interferential electric field distributions based on 2D electrode montage. (a) MEMA values at the central, horizontal edge and vertical edge points. (b) Normalized MEMAs of horizontal and vertical lines. And the definitions of 50% width and 80% width. ($\theta_1 = 30°$, $\theta_2 = 150°$.) (c) 50% and 80% width of horizontal and vertical lines with different return electrode positions. ($\theta_1 = 30°$, θ_2 changed from 90° to 170° with a step of 20°.)

Through the quantitative analysis results, the vertical resolution was significantly improved due to the application of the 3D montage. Meanwhile, the overall resolution of both vertical and horizontal directions was superior to that of the 2D electrode montage. From Fig. 8(c), when θ_2 was greater than 90°, the 50% width existed due to the presence of a focal region in the central retina formed by MEMAs. When θ_2 was 170°, 50% width of both horizontal and vertical directions improved to 10.0°, and 80% width improved to 3.0°. However, 50% width and 80% width in the diagonal direction were 12.0° and 3.7°, respectively, which were worse than these in other directions. The electric field distribution was anisotropic, in which the best resolution appeared at the direction of the electrode placement. Fig. 9 shows the best and worst electric field resolutions of different directions based on 2D and 3D electrode montages. Values under circumstance that central peak value was greater than edge values were chosen, whereas others were masked. Thus, 90° and 110° in vertical direction with 2D montage was missing. 80% width in the horizontal direction was larger than that in the diagonal direction of the 3D electrode montage with the same θ_2 step. The result revealed that the best resolution of the 2D electrode montage was inferior than the worst resolution of the 3D montage. Therefore, in addition to the position of return electrodes, the electrode montage, which also represented the number of electrodes, exhibited a significant effect on the electric field convergence.

C. Steerability of Temporally Interfering Electric Fields With Fixed Electrodes

When the placement of electrodes was fixed, the temporally interfering electric field distributions with different current ratios could be calculated. By means of setting the current ratio appropriately, the interferential electric fields could be controllable and targeted to a specific location of retina. As shown in results above, the convergent electric filed region could be formed on the retinal surface with proper electrode montages. In this study, the electric field steerability was investigated

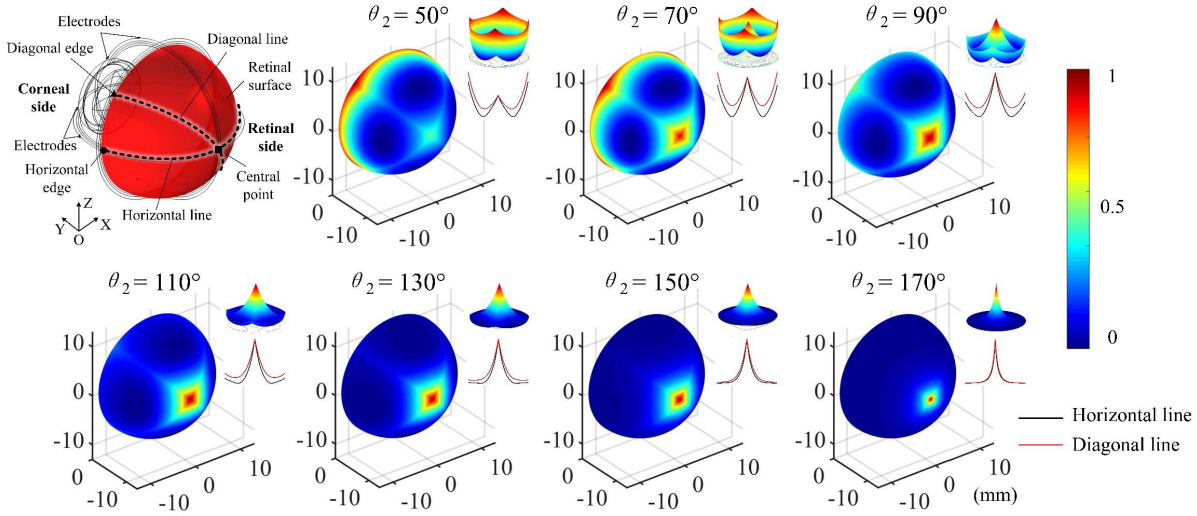

Fig. 7. Normalized interferential electric fields of retinal surface with 3D different electrode montages. ($\theta_1 = 30°$, θ_2 changed from 50° to 170° with a step of 20°. Upper right: 3D mesh diagrams of MEMAs projected to XOZ plane from retinal surface; lower right: normalized MEMAs of horizontal line and diagonal line.)

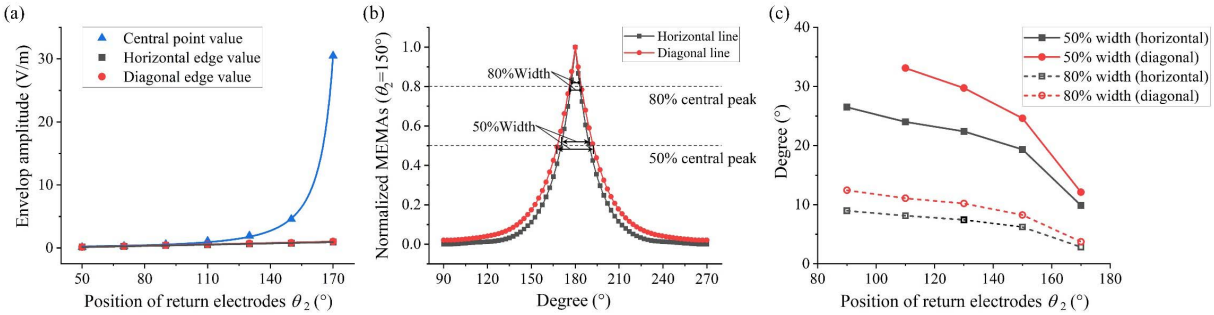

Fig. 8. Quantitative analysis of interferential electric field distributions based on 3D electrode montage. (a) MEMA values at the central, horizontal edge and diagonal edge points. (b) Normalized MEMAs of horizontal and diagonal lines and the definitions of 50% width and 80% width. ($\theta_1 = 30°$, $\theta_2 = 150°$.) (c) 50% and 80% width of horizontal and diagonal lines with different positions of return electrodes. ($\theta_1 = 30°$, θ_2 changed from 90° to 170° with a step of 20°.)

based on the 3D electrode montage with θ_2 fixed at 130°, 150°, and 170° due to their good convergence from results above. Two current ratios (α_x and α_y) were defined and changed. Each of them separately controlled the horizontal or vertical current ratio, which could modulate the targeted site moved to cover the retina surface. Herein, the case when return electrodes were fixed at 150° was taken as an example (Fig. 10) to evaluate the interferential electric fields with different current ratios. With different current ratios, the electric fields were steerable on the retina. When both α_x and α_y were 0.5, the maximum modulated electric field amplitude existed at the central point of the retina. When the current ratios changed, the high-intensity region moved towards the electrode pairs with less current flowing. When α_x individually decreased, the maximum site shifted left; whereas when α_y individually decreased, the site shifted up. When they both decreased, the focal region shifted upper left. Moreover, the shape of the convergent electric field became irregular. As shown in Fig. 10, 80% range of retinal surface was projected to the XOZ plane with different current ratios in the right column. According to the outline of 80% ranges, the electric fields moved regularly within a certain range on the retina around the central position. Further, the specific positions and shapes of the high-intensity region caused by different current ratios could be detected. The steerability of the electric field was at the expense of the convergence of electric field, which would increase the difficulty of neuromodulation.

In addition, the electric field convergence and steerability with different return electrode placements were compared. Because of the symmetry of electric fields, the mobility of the electric fields over a quarter of the retinal surface was explored. 80% range of the interferential electric field was projected in a quarter circle of the XOZ plane in Fig. 11. Under different current ratio parameters, the central position of each small circle represented the projected position with the strongest intensity of electric field. The size of each circle was one-third area of the retinal arc surface covered within the 80% range, and the color displayed different MEMA values corresponding to the color bar on the right. In Fig. 11(a)-(c), the difference between electric field steerability and convergence with different return electrode placements was visually compared. When the position of the return electrodes was fixed, the position

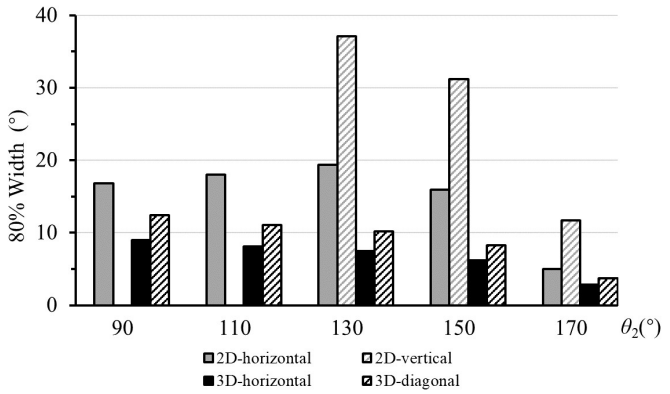

Fig. 9. The 80% width of horizontal and vertical/diagonal line with different positions of return electrodes in 2D and 3D electrode montage. ($\theta_1 = 30°$, θ_2 changed from 90° to 170° with a step of 20°.)

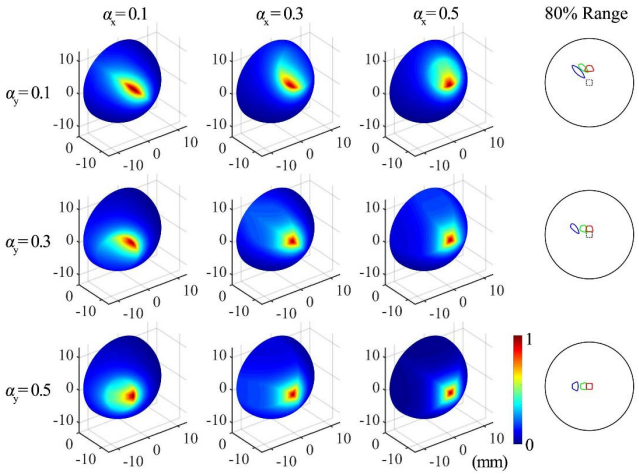

Fig. 10. Steerability of the interferential electric fields with different current ratios based on 3D electrode montage when θ_2 was 150°. Three columns on the left: the MEMAs of retinal surface with α_x and α_y changing from 0.1 to 0.5; right column: 80% range of high intensity electric fields projected to 2D XOZ plane.

of circle center changed with the variation of the current ratio. Moreover, the steerable range of the circle center was distinct at different electrode positions. With the increasing θ_2, the steerable range became smaller. Besides, the peak offset was plotted, which was defined as the angle between the strongest peak position under certain current ratios and the peak position when α_x and α_y equaling 0.5 of horizontal and diagonal lines, as shown in Fig. 11(d) and (e). It was found that when α_x individually changed, which meant the high intensity region shifted on the horizontal line, the peak offset and current ratio with the same electrode placement fitted well to the quadratic curve. When the return electrodes located at 130°, the peak offset was the largest, and it could target the largest range of the retina. Moreover, its unilateral largest steerable range was about 40°. When both α_x and α_y were changed and the high-intensity region moved in the diagonal direction, the peak offset kept rising, but the regularity was not as good as that in the horizontal direction. According to results of the linear fitting, the steerable range also reached the largest, approximately 50°, when θ_2 was 130°.

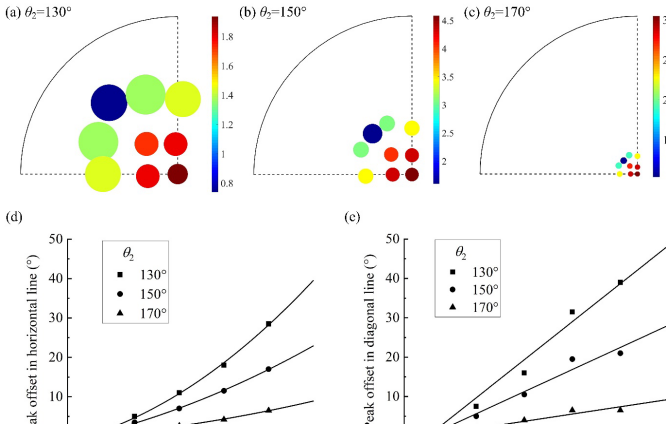

Fig. 11. The steerability of interferential electric fields with different current ratios and return electrode positions. (a)-(c) The projected 80% range of the interferential electric fields from retinal surface to a quarter circle of the XOZ plane due to the symmetry of electric fields. The center position of each small circle represented the projected position of the electric field peak, where α_x and α_y were changed from 0.1 to 0.5 in a step of 0.2. The size of each circle was 1/3 of the area of the arc surface of the retina covered within 80% range and the color showed different MEMA values. (d) Peak offset in horizontal line with α_x changing from 0.5 to 0.1. ($\theta_2 = 130°$, 150°, 170°) (e) Peak offset in diagonal line with α_x and α_y changing from 0.5 to 0.1. ($\theta_2 = 130°$, 150°, 170°.)

By comparing the circle color in each picture, it was found that the electric field intensity decreased as the current ratio changed from 0.5 to 0.1. The peak of the electric field at the outermost edge was about half the peak at the center. In addition, the size of the circles in different figures was compared. Under the same electrode placement, the circle area at the center position was the smallest, which meant the electric field obtained the strongest convergence and precision of the regulation. As the current ratio decreased, the area of the circles increased. However, the increasing relationship between the circle area and the current ratio was not monotone. As such, when θ_2 was 130°, the area of the circle with α_x and α_y equaling 0.1 was smaller than that with α_x was 0.3 and α_y was 0.1. This might cause by the variation of the shape of the high-intensity region, which became irregular. Therefore, when the stimulating range and precision of the interferential electric fields with different current ratios were taken into consideration, the shape and area of the stimulating region should be investigated comprehensively.

IV. Discussion

In this study, an electrical conductivity model of the eyeball and multiple extraocular electrodes was established. Electrode pairs were symmetrically distributed around the eye, passed the sinusoidal current with both identical and various intensity with different frequencies, and stimulated the retina by TI strategy. According to the modeling results, it could be concluded that TI stimulation with appropriate electrode montages could target a specific area of retinal neurons. Additionally, the focal targeted region could be steerable. Its size and position could be regulated by the placement of electrodes and the current ratio passed by the different stimulating channels.

A. The Influence of Different Electrode Montage on the Distribution of Interferential Electric Field

Temporally interfering electric field distributions with various 2D and 3D electrode montages were simulated. The position of electrodes would strongly affect the distribution. When the return electrodes were located at the retinal side of the eyeball, a focal region with high intensity of electric fields would be formed on the central retina. Moreover, the range of this region would decrease, and its amplitudes would significantly increase when the return electrodes got close to the retinal side. As shown in Fig. 4, electric fields not uniformly distributed in the eye model, whereas they were mutated at the interface of different tissues due to different conductivities of various eye structures. Based on the principle of interferential stimulation, the region around the midperpendicular of stimulating or return electrodes obtained a higher consistency and alignment of electric field distribution. Therefore, the interferential electric fields within this range were higher after superposition. Furthermore, the position of stimulating electrodes around the anterior side of the eyeball was also changed. And the electric fields in the cornea, atria, and lens were greatly affected, whereas the targeted retina was less affected as shown in *Supplemental Information* section A. Thus, θ_2 equaling to 30°, which was near the edge of the cornea, was selected as the typical position of stimulating electrodes in order not to cause additional damage to the corneal tissue [23].

Apart from changing the position of the electrodes, increasing the electrode numbers could improve the resolution of electric field. The 3D electrode montage exhibited better spatial resolution than that of the 2D electrode montage. Based on the 3D electrode montage, the smallest target size of 50% width of in horizontal and vertical direction was 10°, about 2×2 mm^2 size of retinal cube region. 80% width was about 0.6×0.6 mm^2 in this case. In addition, the shape of the high-intensity regions was irregular. When the 2D montage with electrodes placed on the horizontal plane was applied, the produced focal region on the retina was oval-shaped, which exhibited the best resolution in the horizontal direction but the poor resolutions in others. When the 3D montage with electrodes distributed in both vertical and horizontal directions was performed, the best resolutions appeared at both horizontal and vertical directions. Therefore, the formed high-intensity region was square-shaped. It indicated the capability to improve the resolution in particular direction or regulate the targeted shape by adjusting electrode montages in specific direction. Meanwhile, the increased number of electrodes could enhance the resolution, allowing for more fine-grained modulation of retinal neurons. Whereas it also increased the complexity of electrode and trauma.

The results in this study were consistent with those of Grossman *et al.*, which enabled spatially selective stimulation of neurons deep in the brain [16]. But differently, in this study, spatially selective stimulation of retinal neurons distributed near the eyeball surface was investigated and a larger area was covered. Therefore, it is necessary to keep the return electrode pairs closer to the retinal side, different from the DBS electrode montage. Therefore, different electrode montages met the needs of distinct stimulations.

B. The Steerability of Focal Region by Changing the Current Ratios

The steerability of the high-intensity focal region was studied as well. The results revealed that the position of this focal region could be regulated by altering the current ratios passed by different electrode channels. Consequently, a large range of neurons could be stimulated in different locations with a limited number of electrodes. For the 3D electrode montage, the region could move around the retinal surface in both horizontal and vertical directions, which covered a wide range of retinal neurons. However, the shift of interferential electric fields compromised the convergence. Because the TI stimulation was relied on the consistency of electric fields, the high-intensity region would change larger and become unregularly when current ratios were changed. This might increase the difficulty and complexity of control and modulation. Further, the centroid of the high-intensity region would considerably move with current ratios. The maximum steerable range in the 3D montage was about 50° when θ_2 was 130° as shown in Fig. 11, approximately corresponding to the 50° field of vision.

The steerable electric fields controlled by current ratios without physical electrode movability were similar to the concept of virtual electrodes, which was firstly applied in cochlear implants [29] and utilized for retinal prostheses currently [22], [30], [31]. But unlike the traditional virtual electrodes achieved by direct superposition of the electric field intensity, the movable direction of the interferential electric fields induced by the superposition of various current with different frequencies and amplitudes was closer to electrode pairs with the less output current. However, the traditional virtual electrodes moved closer to the electrode side with a higher output current [22], which can be attribute to distinct principles of the stimulation strategy.

C. The Choice of Frequency in the TI Stimulation

The choice of stimulus frequency, of both the carrier and difference frequencies, was a significant factor during retinal stimulation with temporally interfering electrical field. To date, there have been no specific study exploring the response of retinal neurons to TI stimulation. Some research groups have already conducted researches on the response characteristics of retinal neurons induced by electrical stimulation with different sinusoidal frequencies. Freeman *et al.* elicited a retinal response using electrical stimulation with frequencies from 5 to 100 Hz with rabbits *in vitro*. They demonstrated that specific frequencies of sinusoidal stimulation could be utilized to preferentially activate certain retinal cell types: photoreceptors are activated at 5 Hz, bipolar cells at 25 Hz, and ganglion cells at 100 Hz [32]. This shows different types of retina neurons respond to different frequencies. Further study conducted by Twyford *et al.* in the same group confirmed this result, and further revealed that during sinusoidal stimulation,

low frequencies were more efficient than high frequencies [33]. Hadjinicolaou *et al.* reached a similar conclusion with retina of rats *in vitro*. They found that most types of retinal ganglion cells (RGCs) showed the characteristics of a low- or band-pass, with the strongest response to sinusoidal stimuli being within frequencies ranging from 2 to 30 Hz. They determined that sinusoidal stimuli reached a cut-off frequency between 8 and 56 Hz and had a weak or almost no response at higher frequencies [34]. Through modeling, Kameneva *et al.* demonstrated that certain types of retinal bipolar cells were more responsive to sinusoidal stimulation at lower frequencies (2-10Hz), than at higher frequency (100Hz) [35]. In summary, retinal neurons are more responsive to low-frequency sinusoidal electrical stimulation than to high-frequencies, which is similar to what was determined experimentally for brain neurons [16]. However, some researches demonstrated that retinal neurons do response to high-frequency stimulation. Cai *et al.* and Twyford *et al.* in the same group demonstrated that various types of RGCs exhibited a non-monotonic, stimulus-strength-dependent response during high-frequency (2 kHz) biphasic electrical stimulation with rabbit retina *in vitro* [36], [37], which was different from those elicited by other electrical stimuli. This phenomenon has been extensively studied because of its potential indications for targeting certain functionally distinct RGC types without simultaneously producing any significant response in others [38], [39]. Kameneva *et al.* believed that differences in transmembrane potassium conductance, which leaded to different depolarization block patterns, explained this phenomenon [38]. Whereas Guo *et al.* suggested that the phenomenon was due to local membrane hyperpolarization caused by outward membrane currents near the stimulus electrode [39]. Therefore, further studies are required to better understand the factors that shape the responses of distinct retinal neurons to high-frequency stimulation. This spike inhibition during TI stimulation might generate unwanted side effects. However, a similar inhibition phenomenon, called "conduction block", was also observed in deep brain stimulation with TI strategy. The study showed that the conduction block would occur in the regions of low or no envelope modulation, and would in general, not affect the response in the targeted region [40]. Besides, variations in the excitability characteristics of retinal cells and their neuronal substructures depend on not only on cell type but also on the region [41]. However, the latest research showed that the previously proposed mechanism of passive membrane low-pass filtering was insufficient for TI excitation [16]. Instead, an active ion-channel mediated signal ratification process allowed neurons to respond to TI stimulation. TI excitation neural mechanism has not been investigated on retinal neurons. However, the phenomenon of the response to envelope stimuli was consistent with that of DBS [16]. Kelbsch *et al.* induced pupillary responses by enveloping-sinusoidal TES and found that the pupillary reflex followed the frequency of the enveloping waveform rather than the carrier frequency [42]. Thus, from the perspective of the performance of the visual system, we suspected that the visual response under enveloping-sinusoidal stimulation followed the enveloping frequency, rather than the carrier frequency. Thus, in future modeling and experimental studies, TI should be applied to the physiological retinal neurons to further verify the physiological feasibility and limitations. Based on a combination of the discussion above and the results of previous researched, it is probable that TI stimulation does not work on all types of retinal neurons [20], [40]. This suggest that great care should be taken when applying TI stimulation to retina, where multiple neuron-types coexist. Consequently, there is therefore a chance of selective stimulation based on neuron-type, which is a tendency in the development of retinal prosthesis [33], [38], [39].

As mentioned in Section II, the envelope modulation amplitude was calculated under quasi-static conditions. Thus, instead of frequency, only the amplitude of the stimulation influenced the results of the physical modeling. Thus, no specific frequency was specified in the present study. However, the selection of carrier frequencies and difference frequency would determine the envelope modulation waveform, which was of vital significance. This is because the interferential stimulation would further determine the excitation of the retinal neurons. Consequently, the carrier frequency needed to be sufficiently high for the retinal neurons to exhibit TI stimulation [16], [20], i.e. kilohertz. Besides, considering some types of RGC do response to 2 kHz stimulation [36], [37], the carrier frequency might be set above 2 kHz. The difference frequency needed to fall at the optimal response frequency of the targeted neurons [16] and based on previous studies of the retina neurons was from 5 to 100 Hz [32], [34], [35]. Moreover, in the further physiological modeling and *in vitro* as well as *in vivo* studies, it was necessary to consider not only the overall response pattern of the retina, but also the response characteristics of certain types of retinal neurons. This would have important implications for TI stimulation strategy.

D. The Safety of the TI Stimulation

In addition, safety was also an important criterion for TI strategy. During the experiment, the identical input current was applied to various electrode montages to control the variable, which led to large variability of the interferential electric field amplitude. For the safety of electrical stimulation, the electrode montages that could generate stronger electric field intensity with the same input current would be chosen in further experiments. Meanwhile, as the variation of the input current would not alter the response regularity of the electric field, the input of a relatively small current through the selected electrode montage could help the electric field at the retina reach the response threshold of neurons in practical applications. Besides, as shown in *Supplemental Information* section B, the electrode size correlated with the upper limit of charge injection at the electrode-tissue interface had little impact on the electric field distribution of the retina [43]. Thus, both aspects made it easier to achieve the modulation of retinal neurons under the limitation of charge safety of electrode materials, to ensure the performance of interferential electrical stimulation as well as the life of the electrode. As shown in *Results*, as the number of electrodes increased, and the return electrodes became closer to the retinal side of the eyeball, the convergence of electric field increased, which was at the

expense of increasing invasiveness to the eye structure. The results also showed that as the return electrodes got closer, the amplitude of interferential electric fields on the retina greatly increased, which gave rise to decrease the current threshold of the retinal stimulation strategy. Moreover, the threshold evoked by sinusoidal stimulation was lower than that of commonly-used rectangular stimulation [29], [44]. However, it has been reported that the RP patients had a higher perceptive threshold than normally sighted people [45]. Thus, further *in vivo* studies are needed to explore the actual current threshold and appropriate stimulating current with specific electrode material and montage.

E. The Comparison of Three Approaches for Retinal Electrical Stimulation

The comparison of characteristics regarding TES, retinal prostheses and TI stimulation is expounded. TES delivers electrical currents to the retina via contact lens electrodes attached to the corneal surface [1]. Retinal prostheses directly stimulate retinal neurons via the intraocular electrode array [46]. And TI stimulation activates retinal neurons via multiple extraocular electrodes with interferential electric fields.

In terms of the spatial resolution of the stimulations, TES would mainly stimulate the peripheral retina, without spatial selectivity and convergence [1], whereas TI stimulation and retinal prosthesis could spatially and selectively stimulate local retinal region with certain convergence. Theoretically speaking, the spatial resolution of the retinal prosthesis depends on the electrode size and interelectrode spacing [43], And that of TI stimulation rests upon the sharpness of the interferential electric field distribution curve, which could activate retinal neuron, at specific retinal region under certain electrode montage, as shown in Fig. 7. Within the stimulation range of this electrode montage, the generated stimulus points are continuous via varying current ratios of different stimulation channels, which differs from the retinal prosthesis limited by the spacing of adjacent electrodes [43]. And by increasing the number of electrode channels, developing more sophisticated electrode montages and various stimulation strategies in further study, TI strategy with multisite and steerable stimulation would be promising for retinal prosthesis [20]. Besides, according to the change principle of the electric field distribution, the convergence is the best at the central region, and when the stimulus site moving to the edge of the stimulation range, the focal region would change larger and become unregular with the same stimulation intensity. Thus, the spatial resolution of TI stimulation is varied from high to low, as the stimulus site moved from the center to the periphery. Unlike the stimulus sites generated by retinal prosthesis is same size and equally distributed with constant spatial resolution. However, visual acuity diminishes from the center to the periphery of the retina [47]. Thus, the patterns generated by TI stimulation is much more in line with the physiological characteristics of retina.

Besides, a different aspect of stimulation effects, equally pivotal to the spatial resolution, is the stimulation range. TES would primarily stimulate the peripheral retina. For the sake of full restoration of the normal visual field, the electrode array of retinal prosthesis should cover the entire retina [43]. However, the actual size of the array is strictly limited by physiological, surgical and mechanical considerations [43]. Commercial-used retinal prostheses, Argus II and Alpha IMS implant, cover a maximum diagonal visual angle of 22° and 15°, respectively. Under TI stimulation, the centroid of the high-intensity region could considerably move with current ratios as shown in Fig. 11. The maximum steerable range in the 3D montage is about 100° in the diagonal direction when θ_2 is 130°, approximately corresponding to the 50° diagonal visual angle. However, as aforementioned, the shift of interferential electric fields compromises the stimulating spatial resolutions, which might add to the difficulty and complexity of control and modulation.

Last but not the least, there is a need to discuss invasiveness as well. Although the invasiveness of TI stimulation is larger than that of TES [1], the extraocular position of the implanted electrode array would greatly lower the physical damage to the eye when compared with retinal prosthesis. Considering that the incision on the eyeball as retinal prostheses is not required, the probability of endophthalmitis as well as retinal hemorrhage was diminished, which are major severe adverse events of the surgery for retinal prostheses [48]. Besides, the implanted part might require removal at the conclusion of clinical trials [49]. Thus, the safety and efficacy of explanting the extraocular implant of TI stimulation was more reliable than the intraocular implant of retinal prostheses.

V. Conclusion

To sum up, a multi-electrode retinal stimulation model was proposed to explore the feasibility of spatially selective retinal stimulation, which was based on temporally interfering electric fields with different electrode montages and current ratios. The results suggested the TI stimulation with appropriate electrode montages could target a specific region of retinal neurons. The focal targeted region was also steerable, and its size and position could be regulated by the placement and position of electrodes together with the current ratio passed by the stimulating channels. It could be concluded that the local retinal region could be stimulated spatially and selectively by temporally interfering electrical stimulation with certain convergence and a relatively large stimulation range, which would be instructive for the study of a novel retinal neuromodulation method, and further benefit for the retinal locoregional electrostimulation as well as the innovative design of visual functional restoration. However, only the theoretical physical feasibility was validated with the custom multi-electrode retinal stimulation model, which increased the necessity of implementing further investigation with neural modeling and *in vivo* experiments to explore the appropriate stimulation parameters and testify its physiological and clinical feasibilities.

References

[1] A. Sehic, S. Guo, K.-S. Cho, R. M. Corraya, D. F. Chen, and T. P. Utheim, "Electrical stimulation as a means for improving vision," *Amer. J. Pathol.*, vol. 186, no. 11, pp. 2783–2797, Nov. 2016.

[2] Z. Ma *et al.*, "Optical imaging of visual cortical responses evoked by transcorneal electrical stimulation with different parameters," *Investigative Ophthalmol. Vis. Sci.*, vol. 55, no. 8, pp. 5320–5331, Aug. 2014.

[3] P. Sun *et al.*, "Comparison of cortical responses to the activation of retina by visual stimulation and transcorneal electrical stimulation," *Brain Stimulation*, vol. 11, no. 4, pp. 667–675, Jul./Aug. 2018.

[4] A. Y. Chow, V. Y. Chow, K. H. Packo, J. S. Pollack, G. A. Peyman, and R. Schuchard, "The artificial silicon retina microchip for the treatment of visionloss from retinitis pigmentosa," *Arch. Ophthalmol.*, vol. 122, no. 4, pp. 460–469, Apr. 2004.

[5] T. Morimoto, H. Kanda, M. Kondo, H. Terasaki, K. Nishida, and T. Fujikado, "Transcorneal electrical stimulation promotes survival of photoreceptors and improves retinal function in rhodopsin P347L transgenic rabbits," *Investigative Ophthalmol. Vis. Sci.*, vol. 53, no. 7, pp. 4254–4261, Jun. 2012.

[6] A. Schatz *et al.*, "Transcorneal electrical stimulation for patients with retinitis pigmentosa: A prospective, randomized, sham-controlled exploratory study," *Investigative Ophthalmol. Vis. Sci.*, vol. 52, no. 7, pp. 4485–4496, Jun. 2011.

[7] T. Kurimoto, S. Oono, R. Kashimoto, Y. Tagami, N. Okamoto, and O. Mimura, "Transcorneal electrical stimulation improves visual function in eyes with branch retinal artery occlusion," *Clin. Ophthalmol.*, vol. 5, p. 397, Mar. 2011.

[8] X. Wang *et al.*, "Neuroprotective effect of transcorneal electrical stimulation on ischemic damage in the rat retina," *Exp. Eye Res.*, vol. 93, no. 5, pp. 753–760, Nov. 2011.

[9] P. Henrich-Noack, N. Voigt, S. Prilloff, A. Fedorov, and B. A. Sabel, "Transcorneal electrical stimulation alters morphology and survival of retinal ganglion cells after optic nerve damage," *Neurosci. Lett.*, vol. 543, pp. 1–6, May 2013.

[10] A. Schatz *et al.*, "Transcorneal electrical stimulation shows neuroprotective effects in retinas of light-exposed rats," *Investigative Ophthalmol. Vis. Sci.*, vol. 53, no. 9, pp. 5552–5561, Aug. 2012.

[11] J. Xie *et al.*, "Modeling and percept of transcorneal electrical stimulation in humans," *IEEE Trans. Biomed. Eng.*, vol. 58, no. 7, pp. 1932–1939, Jul. 2011.

[12] T. Morimoto *et al.*, "Evaluation of residual retinal function by pupillary constrictions and phosphenes using transcorneal electrical stimulation in patients with retinal degeneration," *Graefe's Arch. Clin. Exp. Ophthalmol.*, vol. 244, no. 10, p. 1283, Oct. 2006.

[13] D. Yana *et al.*, "The value of preoperative tests in the selection of blind patients for a permanent microelectronic implant," *Trans. Amer. Ophthalmol. Soc.*, vol. 101, pp. 43–50, 2004.

[14] Q. Huang, V. Chowdhury, and M. T. Coroneo, "Evaluation of patient suitability for a retinal prosthesis using structural and functional tests of inner retinal integrity," *J. Neural Eng.*, vol. 6, no. 3, May 2009, Art. no. 035010.

[15] G. C. Goats, "Interferential current therapy," *Brit. J. Sports Med.*, vol. 24, no. 2, p. 87, 1990.

[16] N. Grossman *et al.*, "Noninvasive deep brain stimulation via temporally interfering electric fields," *Cell*, vol. 169, no. 6, pp. 1029.e16–1041.e16, Jun. 2017, doi: 10.1016/j.cell.2017.05.024.

[17] M. Agharezaee and A. Mahnam, "A computational study to evaluate the activation pattern of nerve fibers in response to interferential currents stimulation," *Med. Biol. Eng. Comput.*, vol. 53, no. 8, pp. 713–720, Apr. 2015.

[18] K. A. Caulfield and M. S. George, "The future of brain stimulation treatments," *Psychiatric Clinics*, vol. 41, no. 3, pp. 515–533, Sep. 2018.

[19] X. Chai, J. Guo, and H. Li, "An extraocular electrode array device for spatially selective electrical stimulation of the retina," Chinese Patent CN110270009A, Sep. 24, 2019.

[20] J. Cao and P. Grover, "STIMULUS: Noninvasive dynamic patterns of neurostimulation using spatio-temporal interference," *IEEE Trans. Biomed. Eng.*, vol. 67, no. 3, pp. 726–737, Mar. 2020.

[21] F. Karimi, A. Attarpour, R. Amirfattahi, and A. Z. Nezhad, "Computational analysis of non-invasive deep brain stimulation based on interfering electric fields," *Phys. Med. Biol.*, vol. 64, no. 23, Dec. 2019, Art. no. 235010.

[22] Q. Lyu *et al.*, "A three-dimensional microelectrode array to generate virtual electrodes for epiretinal prosthesis based on a modeling study," *Int. J. Neural Syst.*, vol. 30, no. 3, Mar. 2020, Art. no. 2050006.

[23] M. Cvetkovic, D. Cavka, and D. Poljak, "A simple finite element model of heat transfer in the human eye," in *Proc. Int. Conf. Softw. Telecommun. Comput. Netw.*, 2006, pp. 27–31.

[24] S. Gabriel, R. W. Lau, and C. Gabriel, "The dielectric properties of biological tissues: III. Parametric models for the dielectric spectrum of tissues," *Phys. Med. Biol.*, vol. 41, no. 11, p. 2271, 1996.

[25] C. Cela, "A multiresolution admittance method for large-scale bioelectromagnetic interactions," Ph.D. dissertation, Dept. Elect. Eng., NC State Univ., Raleigh, NC, USA, 2010.

[26] J. Y. Won, S. E. Kim, and Y.-H. Park, "Effect of age and sex on retinal layer thickness and volume in normal eyes," *Medicine*, vol. 95, no. 46, p. e5441, Nov. 2016.

[27] R. E. Norman, J. G. Flanagan, I. A. Sigal, S. M. K. Rausch, I. Tertinegg, and C. R. Ethier, "Finite element modeling of the human sclera: Influence on optic nerve head biomechanics and connections with glaucoma," *Exp. Eye Res.*, vol. 93, no. 1, pp. 4–12, Jul. 2011.

[28] R. Plonsey and D. B. Heppner, "Considerations of quasi-stationarity in electrophysiological systems," *Bull. Math. Biophys.*, vol. 29, no. 4, pp. 657–664, Dec. 1967.

[29] Y. Nakano *et al.*, "Sinusoidal electrical pulse more efficiently evokes retinal excitation than rectangular electrical pulse in retinal prostheses," *Sens. Mater.*, vol. 29, no. 12, pp. 1667–1677, 2017.

[30] G. Dumm, J. B. Fallon, C. E. Williams, and M. N. Shivdasani, "Virtual electrodes by current steering in retinal prostheses," *Investigative Ophthalmol. Vis. Sci.*, vol. 55, no. 12, pp. 8077–8085, Dec. 2014.

[31] T. C. Spencer, J. B. Fallon, and M. N. Shivdasani, "Creating virtual electrodes with 2D current steering," *J. Neural Eng.*, vol. 15, no. 3, Mar. 2018, Art. no. 035002.

[32] D. K. Freeman, D. K. Eddington, J. F. Rizzo, and S. I. Fried, "Selective activation of neuronal targets with sinusoidal electric stimulation," *J. Neurophysiol.*, vol. 104, no. 5, pp. 2778–2791, Nov. 2010.

[33] P. Twyford and S. Fried, "The retinal response to sinusoidal electrical stimulation," *IEEE Trans. Neural Syst. Rehabil. Eng.*, vol. 24, no. 4, pp. 413–423, Apr. 2016.

[34] A. E. Hadjinicolaou, S. L. Cloherty, Y.-S. Hung, T. Kameneva, and M. R. Ibbotson, "Frequency responses of rat retinal ganglion cells," *PLoS ONE*, vol. 11, no. 6, Jun. 2016, Art. no. e0157676.

[35] T. Kameneva, D. B. Grayden, and A. N. B. H. Meffin, "Sinusoidal stimulation of retinal bipolar cells: A modelling study," in *Proc. 9th IASTED Int. Conf. Biomed. Eng.*, 2012, vol. 9, no. 1, pp. 389–394.

[36] C. Cai, P. Twyford, and S. Fried, "The response of retinal neurons to high-frequency stimulation," *J. Neural Eng.*, vol. 10, no. 3, Jun. 2013, Art. no. 036009.

[37] P. Twyford, C. Cai, and S. Fried, "Differential responses to high-frequency electrical stimulation in ON and OFF retinal ganglion cells," *J. Neural Eng.*, vol. 11, no. 2, Apr. 2014, Art. no. 025001.

[38] T. Kameneva *et al.*, "Retinal ganglion cells: Mechanisms underlying depolarization block and differential responses to high frequency electrical stimulation of ON and OFF cells," *J. Neural Eng.*, vol. 13, no. 1, Feb. 2016, Art. no. 016017.

[39] T. Guo *et al.*, "Mediating retinal ganglion cell spike rates using high-frequency electrical stimulation," *Frontiers Neurosci.*, vol. 13, p. 413, Apr. 2019.

[40] E. Mirzakhalili, B. Barra, M. Capogrosso, and S. F. Lempka, "Biophysics of temporal interference stimulation," *Cell Syst.*, vol. 11, no. 6, pp. 557–572, Dec. 2020.

[41] A. E. Hadjinicolaou, P. Werginz, J.-I. Lee, and S. I. Fried, "Differential responses to high-frequency electrical stimulation in brisk-transient and delta retinal ganglion cells," in *Proc. 42nd Annu. Int. Conf. IEEE Eng. Med. Biol. Soc. (EMBC)*, Jul. 2020, pp. 3529–3532.

[42] C. Kelbsch *et al.*, "Phosphene perception and pupillary responses to sinusoidal electrostimulation–for an objective measurement of retinal function," *Exp. Eye Res.*, vol. 176, pp. 210–218, Nov. 2018.

[43] L. Yue, J. D. Weiland, B. Roska, and M. S. Humayun, "Retinal stimulation strategies to restore vision: Fundamentals and systems," *Prog. Retinal Eye Res.*, vol. 53, pp. 21–47, Jul. 2016.

[44] A. C. Weitz *et al.*, "Improving the spatial resolution of epiretinal implants by increasing stimulus pulse duration," *Sci. Transl. Med.*, vol. 7, no. 318, Dec. 2015, Art. no. 318ra203.

[45] J. Xie *et al.*, "Preservation of retinotopic map in retinal degeneration," *Exp. Eye Res.*, vol. 98, pp. 88–96, May 2012.

[46] L. N. Ayton *et al.*, "An update on retinal prostheses," *Clin. Neurophysiol.*, vol. 131, no. 6, pp. 1383–1398, Jun. 2020, doi: 10.1016/j.clinph.2019.11.029.

[47] F. N. Low, "Peripheral visual acuity," *Arch. Ophthalmol.*, vol. 45, no. 1, pp. 80–99, Jan. 1951.

[48] J. D. Weiland and M. S. Humayun, "Retinal prosthesis," *IEEE. Trans. Biomed. Eng.*, vol. 61, no. 5, pp. 1412–1424, May 2014.

[49] R. T. Leung *et al.*, "Safety and efficacy of explanting or replacing suprachoroidal electrode arrays in a feline model," *Clin. Experim. Ophthalmol.*, vol. 43, no. 3, pp. 247–258, Apr. 2015.